Evaluating the Effects of Inlet Geometry on the Limiting Flux of Secondary Settling Tanks with CFD Model and 1D Flux Theory Model

Haiwen Gao[1] and M. K. Stenstrom, Ph.D., F.ASCE[2]

Abstract: The effects of the McKinney baffle on the limiting flux of secondary settling tanks (SSTs) are evaluated by comparing the predictions of the maximum solids loading rate (SLR) determined by a Fluent-based, two-dimensional computational fluid dynamics (CFD) model with limits calculated by one-dimensional idealized flux theory (1DFT). SLR stress tests are simulated using three different stress testing methods to adjust flow rate, SLR, recycle ratio, and concentration of mixed liquor suspended solids. For each method, different flow conditions are used as the starting points for the CFD stress test. Limiting fluxes of the SST without and with the McKinney baffle are compared, and the SSTs failure mechanisms are analyzed. The simulations show that the McKinney baffle improves SST limiting flux by 1.4–2 times over the limiting of the original SST. Also, different (1) baffling structures; (2) stress testing methods; and (3) initial flow conditions for CFD stress tests influence the prediction of the limiting SLR. Therefore, routinely assuming a flux rating of 80% of the 1DFT limit is not recommended for all SSTs. **DOI: 10.1061/(ASCE)EE.1943-7870.0001582.** © *2019 American Society of Civil Engineers.*

Author keywords: McKinney baffle; Computational fluid dynamics; Limiting flux; Secondary settling tank; Computational fluid dynamics (CFD) stress test.

Introduction

The state point analysis (SPA) method developed by Keinath et al. (1977) and Keinath (1985) is one of the most practical approaches to analyze the behavior of existing secondary settling tanks (SSTs) as well as improving the operation of full-scale SSTs (Water Environmental Federation 2006). It is based on one-dimensional flux theory (1DFT), and the flux curve can be easily developed by on-site observations. However, since it simplifies the SSTs to the idealized steady-state 1D model, it ignores the nonideal effects of (1) hydrodynamics, such as turbulence, density currents, flocculation, wind and temperature, and the effects of (2) the arrangement of the internal geometry, such as energy dissipation inlet (EDI), flocculation well, McKinney baffle, Stamford baffle, etc. (Ekama and Marais 2004). Therefore, the actual flux capacities of SSTs are lower than the prediction of the 1DFT and the applications of 1DFT without considering a proper safety factor can cause incorrect design and operation of the SST.

In order to understand the effects of hydrodynamics and the arrangement of internal features on the performance of the SST, computational fluid dynamics (CFD) models have been developed in the last 30 years and have been used to (1) understand the hydrodynamics in the SST (Zhou and McCorquodale 1992a, b, c; McCorquodale et al. 2004); (2) optimize internal structures (Xanthos et al. 2011, 2013); and (3) adjust operation process (Vitasovic et al. 1997; Wahlberg et al. 1998; Ekama and Marais 2004; Parker et al. 2008; Patziger et al. 2012; Gao and Stenstrom 2017) and improve sub-models (Lakehal et al. 1999; De Clercq 2003; Ramalingam et al. 2012; Ramin et al. 2014).

Wahlberg et al. (1998) stated that the limiting flux obtained from 1DFT should be considered a theoretical limit, often greater or much greater than actual capacity. With the help of CFD models, the hydrodynamics of SST and the arrangement of internal features can be optimized, and the actual limiting flux can be increased more closely to the theoretical flux limit.

Ekama and Marais (2004) analyzed the effects of Stamford baffles on SST limiting flux in two different wastewater treatment plants (WWTPs) by using the SettlerCAD program (Zhou et al. 1992). In their study, the operation parameters such as recycle rate (Q_r) and concentration of mixed liquor suspended solids (MLSS) were kept constant. The SST was stressed by increasing the flow rate (Q), which had the effect of increasing the surface overflow rate (SOR) and the solids loading rate (SLR). Their simulation results showed that the difference between the CFD predicted limiting flux of the SST with and without the Stamford baffle was only 2%, and the capacities were both around 80% of the maximum flux limit obtained from 1DFT. Therefore, they concluded that the baffling has only a small influence on the capacity of an SST, and 80% of the maximum flux limit obtained from 1DFT is a reasonable value to apply in the design and operation of full-scale SSTs.

However, since the Stamford baffle is only one of the internal features of an SST, the effect of other internal features on the SST's limiting flux need to be studied before making a final conclusion. Also, since grid specification and refinement of SettlerCAD cannot be changed by the user, the numerical diffusion caused by the grid may result in inaccurate prediction results. Moreover, because all constants in the governing equations are coded in the program and

[1]Ph.D. Student, Dept. of Civil and Environmental Engineering, Univ. of California, Los Angeles, 6805 Boelter Hall, Los Angeles, CA 90095. ORCID: https://orcid.org/0000-0001-7387-2289. Email: haiweng92@g.ucla.edu

[2]Professor, Dept. of Civil and Environmental Engineering, Univ. of California, Los Angeles, 5714 Boelter Hall, Los Angeles, CA 90095 (corresponding author). Email: stenstro@seas.ucla.edu

Note. This manuscript was submitted on December 14, 2018; approved on March 1, 2019; published online on August 6, 2019. Discussion period open until January 6, 2020; separate discussions must be submitted for individual papers. This paper is part of the ***Journal of Environmental Engineering***, © ASCE, ISSN 0733-9372.

cannot be changed by the users, they cannot be used to adjust the prediction results to better calibrate the field measurement.

McCorquodale et al. (2004) developed a quasi-three-dimensional (quasi-3D) SST model and used it to evaluate Ekama and Marais's (2004) recommended "80% of the flux limit calculated by IDFT." He adjusted the operation parameters [Q, SLR, returned activated sludge (RAS) ratio, and MLSS] in two ways: (1) keeping the Q and RAS ratio constant while changing SLR by changing the MLSS concentration; and (2) keeping the RAS ratio and MLSS constant while changing SLR and SOR by increasing flow rate (Q). Their results showed that 80% of the flux limit calculated by the IDFT was an accurate correction factor when adjusting the operation parameters using the second method, whereas the 80% of the flux limit calculated by the 1DFT underpredicted the SST real capacity when adjusting the operation parameters using the first stress testing method.

Because the stress testing methods, geometry of SSTs, sludge settling properties, and CFD programs used by McCorquodale et al. (2004) and Ekama and Marais (2004) were different, it is not surprising that their conclusions were different. Therefore, there is a need to compare the limiting flux predicted by the CFD model and 1DFT using these three different stress testing methods in the same SST, sludge settling properties, and the CFD program.

In this study, a Fluent-based two-dimensional (2D) SST CFD model is used to conduct a series of CFD stress tests. The SSTs of Witney WWTP described in Burt (2010) are simulated. A total of 116 simulations are performed in this study. The objectives of this study are to understand (1) the effects of different stress testing methods and (2) the effect of another internal feature—McKinney baffle—on the limiting flux of two different SSTs.

Methodology

Governing Equations and Boundary Conditions

The commercial CFD code ANSYS Fluent (version 18.2) is used to determine the steady-state, turbulent, and density stratified flow in the circular SSTs. Consistent with the previous research by Gao and Stenstrom (2018a, b), the circular SSTs in this research are also investigated using an axisymmetric approach. For circular SSTs with axisymmetric internal features, this approach can dramatically reduce the computational time without deteriorating the simulation accuracy compared with a three-dimensional (3D) model as shown by Patziger et al. (2012).

The equations describing 2D, unsteady, turbulent, and density stratified flow in a circular SST are as follows:

$$\frac{\partial \mathrm{ru}}{\partial \mathrm{r}} + \frac{\partial \mathrm{rv}}{\partial \mathrm{y}} = 0 \qquad (1)$$

r-direction momentum component:

$$\frac{\partial \mathrm{u}}{\partial \mathrm{t}} + \mathrm{u}\frac{\partial \mathrm{u}}{\partial \mathrm{r}} + \mathrm{v}\frac{\partial \mathrm{u}}{\partial \mathrm{y}} = -\frac{1}{\rho}\frac{\partial \mathrm{p}}{\partial \mathrm{r}} + \frac{1}{\mathrm{r}}\frac{\partial}{\partial \mathrm{r}}\left[\mathrm{r}(\vartheta + \vartheta_{\mathrm{t}})\frac{\partial \mathrm{u}}{\partial \mathrm{r}}\right] + \frac{1}{\mathrm{r}}\frac{\partial}{\partial \mathrm{y}}\left[\mathrm{r}(\vartheta + \vartheta_{\mathrm{t}})\frac{\partial \mathrm{u}}{\partial \mathrm{y}}\right] + \mathrm{S_u} \qquad (2)$$

y-direction momentum component:

$$\frac{\partial \mathrm{v}}{\partial \mathrm{t}} + \mathrm{u}\frac{\partial \mathrm{v}}{\partial \mathrm{r}} + \mathrm{v}\frac{\partial \mathrm{v}}{\partial \mathrm{y}} = -\frac{1}{\rho}\frac{\partial \mathrm{p}}{\partial \mathrm{y}} + \frac{1}{\mathrm{r}}\frac{\partial}{\partial \mathrm{r}}\left[\mathrm{r}(\vartheta + \vartheta_{\mathrm{t}})\frac{\partial \mathrm{v}}{\partial \mathrm{r}}\right] + \frac{1}{\mathrm{r}}\frac{\partial}{\partial \mathrm{y}}\left[\mathrm{r}(\vartheta + \vartheta_{\mathrm{t}})\frac{\partial \mathrm{v}}{\partial \mathrm{y}}\right] - \mathrm{g}\frac{\rho - \rho_{\mathrm{r}}}{\rho} + \mathrm{S_v} \qquad (3)$$

where

$$\mathrm{S_u} = \frac{1}{\mathrm{r}}\frac{\partial}{\partial \mathrm{r}}\left[\mathrm{r}(\vartheta + \vartheta_{\mathrm{t}})\frac{\partial \mathrm{u}}{\partial \mathrm{r}}\right] + \frac{1}{\mathrm{r}}\frac{\partial}{\partial \mathrm{y}}\left[\mathrm{r}(\vartheta + \vartheta_{\mathrm{t}})\frac{\partial \mathrm{v}}{\partial \mathrm{r}}\right] - 2\frac{\vartheta + \vartheta_{\mathrm{t}}}{r^2}u \qquad (4)$$

$$\mathrm{S_v} = \frac{1}{\mathrm{r}}\frac{\partial}{\partial \mathrm{r}}\left[\mathrm{r}(\vartheta + \vartheta_{\mathrm{t}})\frac{\partial \mathrm{u}}{\partial \mathrm{y}}\right] + \frac{1}{\mathrm{r}}\frac{\partial}{\partial \mathrm{y}}\left[\mathrm{r}(\vartheta + \vartheta_{\mathrm{t}})\frac{\partial \mathrm{v}}{\partial \mathrm{y}}\right] \qquad (5)$$

u and v = mean velocity components in the r (radial) and y (axial) directions, respectively; p = general pressure less the hydrostatic pressure at reference density ρ_r; ρ = density of mixture; g = acceleration of gravity; ϑ = viscosity of the sludge mixture; and ϑ_t = turbulent eddy viscosity. For density-driven flows, the local fluid density is related to the local values of the sediment concentration by the following relationship:

$$\rho = \rho_{\mathrm{r}} + \mathrm{C}\left(1 - \frac{\rho_{\mathrm{r}}}{\rho_{\mathrm{p}}}\right) \qquad (6)$$

in which C = suspended solids (SS) concentration; ρ_p = dry particle density assumed to be 1,450 $\mathrm{kg/m^3}$ (Larsen 1977); ρ_r = reference density (clear water); and ρ = density of the fluid-solid mixture.

The general transport equations for the turbulent kinetic energy (TKE) (k) and the turbulence dissipation rate (ε), of the standard k–ε turbulence model, can be described by Eqs. (7) and (8), respectively:

$$\frac{\partial \mathrm{u}}{\partial \mathrm{t}} + u\frac{\partial k}{\partial r} + v\frac{\partial k}{\partial y} = \frac{\partial}{\partial r}\left[\left(\vartheta + \frac{\vartheta_{\mathrm{t}}}{\sigma_k}\right)\frac{\partial k}{\partial r}\right] + \frac{\partial}{\partial y}\left[\left(\vartheta + \frac{\vartheta_{\mathrm{t}}}{\sigma_k}\right)\frac{\partial k}{\partial y}\right] + G_k + G_b - \rho\varepsilon \qquad (7)$$

and

$$\frac{\partial \mathrm{u}}{\partial \mathrm{t}} + u\frac{\partial \varepsilon}{\partial r} + v\frac{\partial \varepsilon}{\partial y} = \frac{\partial}{\partial r}\left[\left(\vartheta + \frac{\vartheta_t}{\sigma_\varepsilon}\right)\frac{\partial \varepsilon}{\partial r}\right] + \frac{\partial}{\partial y}\left[\left(\vartheta + \frac{\vartheta_t}{\sigma_\varepsilon}\right)\frac{\partial \varepsilon}{\partial y}\right] + C_1\frac{\varepsilon}{k}G_k - \rho C_2\frac{\varepsilon^2}{k} \qquad (8)$$

The turbulent viscosity has the same form as in the SKE model:

$$\vartheta_{\mathrm{t}} = C_\mu\frac{k^2}{\varepsilon} \qquad (9)$$

The dimensionless empirical constants are given the standard values suggested by Rodi (1993): $C_\mu = 0.09$, $C_1 = 1.44$, $C_2 = 1.92$, $\sigma_k = 1.0$, and $\sigma_\varepsilon = 1.3$.

The solids transport equation in the model is

$$\frac{\partial \mathrm{C}}{\partial t} + u\frac{\partial \mathrm{C}}{\partial r} + v\frac{\partial \mathrm{C}}{\partial y} = \frac{1}{r}\frac{\partial}{\partial r}\left[r\left(\vartheta + \frac{\vartheta_{\mathrm{t}}}{\sigma_{\mathrm{r}}}\right)\frac{\partial \mathrm{C}}{\partial r}\right] + \frac{1}{r}\frac{\partial}{\partial y}\left[r\left(\vartheta + \frac{\vartheta_{\mathrm{t}}}{\sigma_{\mathrm{y}}}\right)\frac{\partial \mathrm{C}}{\partial y} - r\mathrm{V_s C}\right] \qquad (10)$$

in which C = concentration of SS; ϑ = viscosity of the sludge mixture; ϑ_t = turbulent eddy viscosity; and σ_r and σ_y= turbulent Schmidt numbers in the r and y directions, respectively. Both of them are assumed to be 0.7 in this study. V_s is the solids settling velocity.

The solids settling velocity is expressed using the Takács et al. (1991) double exponential function, which is

$$V_s = \max(0, V_o(e^{-r_p(C - C_{\min})} - e^{-r_h(C - C_{\min})})) \qquad (11)$$

J. Environ. Eng., 2019, 145(10): 04019065

where V_o = Stokes velocity; and r_p and r_h account for rapidly and poorly settling floc, respectively. The constant $C_{\min}$ is the concentration of non-settleable solids in the effluent of the SST.

The solids rheological model is proposed by Bokil (1972):

$$v = 1 \times 10^{-6} e^{1.386C} \quad \text{for } C \leq 1 \text{ g/L}$$

and

$$v = 2.9 \times 10^{-6} e^{0.322C} \quad \text{for } C \geq 1 \text{ g/L} \tag{12}$$

in which C = concentration of SS.

Velocity inlet boundary condition is applied to inlet and sludge bottom boundaries, which assumes a uniform distribution of all the dependent variables at the boundary face. For the surface outlet, a pressure outlet boundary condition is applied. Using this type of boundary condition, all flow quantities at the outlets are extrapolated from the interior domain. For the free ambient water surface, the rigid-lid approximation for all velocity components with full slip shear condition is assumed (Wang et al. 2008; Tarpagkou and Pantokratoras 2013). And the free surface boundary is treated as a symmetry condition. The solid boundaries are specified as stationary walls with a no-slip-shear condition, and a standard wall function is used with the turbulence models.

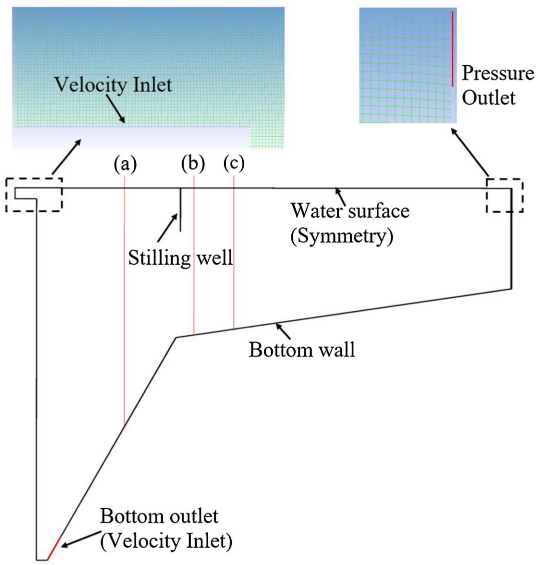

Fig. 1. Original Witney SST diagrams with representative computed locations and boundary conditions. Points (a–c) refer to the radial locations for the grid independent tests and model verification.

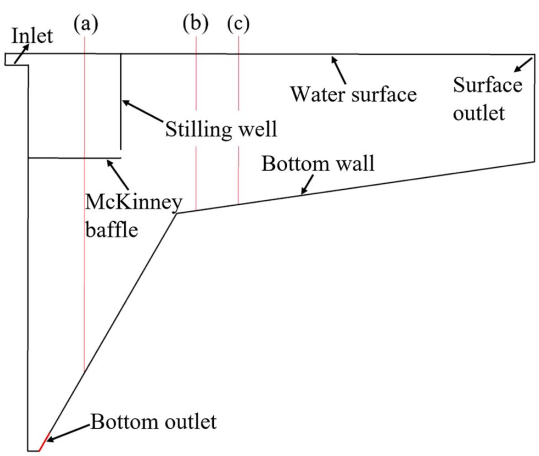

Fig. 2. Modified Witney SST diagrams. Points (a–c) refer to the radial locations for the grid independent tests and model verification.

Geometry and Meshing

The general geometries of original and modified Wintey SSTs and computational meshes with a nearly uniform cell size of 0.00625 × 0.00625 m and approximately 900,000 cells are shown in Figs. 1 and 2, respectively. The radius of the Wintey SST is 18.3 m with a 1.8 m minimum side water depth. The tank floor slope and hopper floor slope are 7.5% and 60%, respectively. Gao and Stenstrom (2018a, 2019) showed the results of mesh-independent tests for the original and modified SSTs, respectively. Because the surface outlet is extremely small compared with the inlet, the meshes near the surface outlet are enlarged in the figure to show the outlet meshes more clearly.

Model Verification

Three different tests (different flow conditions and sludge settling properties) shown in Burt (2010) are used to predict the performance indicators— such as effluent suspended solids (ESS), sludge blanket height (SBH), and the velocity profiles—and to compare with his field measurements. The main inputs for these three tests are shown in Table 1. Fig. 3 shows the CFD model calibration with the field data. The model verification using a medium mesh (428,000 cells) has been completed in Gao and Stenstrom (2019); a larger mesh (approximately 900,000 cells) was used in these simulations and is also accurate.

Stress Test Initialization

Because the model verification studies show that the CFD model results closely fit the observations, the CFD model can be used for the CFD stress tests. For the stress tests, the flow conditions of these three tests are used to initialize the CFD stress tests on each stress testing method used in McCorquodale et al. (2004) and Ekama and Marais (2004). However, the sludge settling properties used in Test 1 are used for all the stress tests to prevent the variation of sludge properties on the prediction of the limiting flux. Therefore, only flow conditions and the internal baffling structure vary

Table 1. Main inputs for the model verification

	Inflow parameters			Settling parameters			Dry solids density
Test no.	MLSS (g/L)	RAS ratio	SOR (m/h)	V_o (m/h)	r_h (L/g)	r_p (L/g)	ρ_p (kg/m^3)
1	4.187	1.09	0.332	12.64	0.340	12.25	1,450
2	3.384	1.09	0.332	13.32	0.386	13.00	1,450
3	2.904	0.83	0.673	13.32	0.386	13.00	1,450

Note: $\boldsymbol{V_o}$ = stokes velocity; and $\boldsymbol{r_h}$ and $\boldsymbol{r_p}$ account for rapidly and poorly settling floc, respectively.

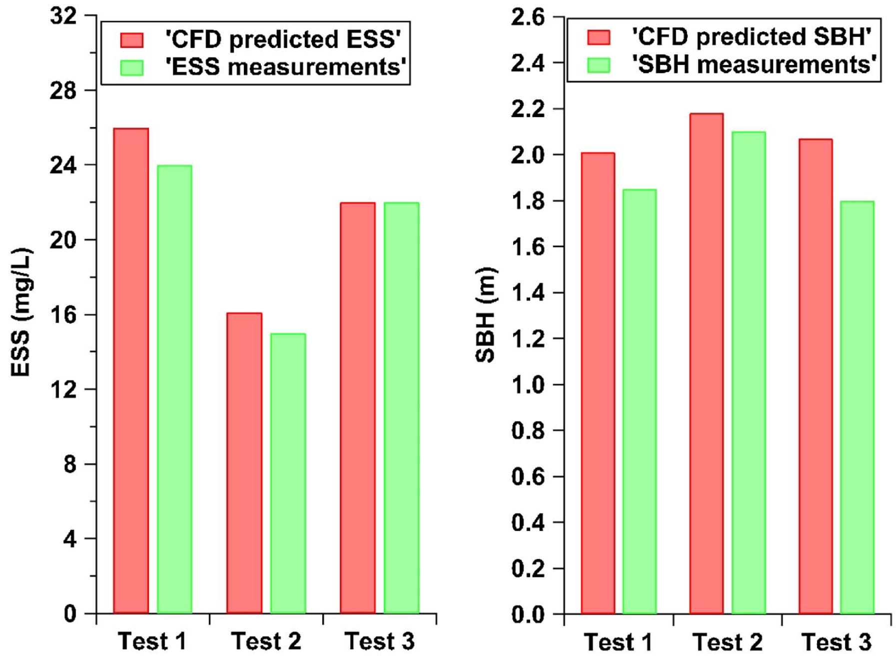

Fig. 3. Comparison between the predictions of performance indicators with the CFD model and field data for the Witney SSTs.

during the CFD stress testing. Table 2 shows the three inputs used for CFD stress tests.

The first stress test method is to increase the SLR and SOR by increasing the flow rate (Q), while keeping the RAS ratio and inlet MLSS concentration constant (McCorquodale et al. 2004). The second stress test method is to increase the SLR and SOR by increasing the flow rate but keeping the returned flow rate (Q_r) and inlet MLSS concentration constant (Ekama and Marais 2004). The third stress method is to increase the SLR by increasing the MLSS concentration, while keeping the influent flow (Q) and recycle flow (Q_r) constant (McCorquodale et al. 2004).

Prediction of the 1DFT Limiting Flux

The 1DFT limiting flux for each stress test method is the same as used by McCorquodale et al. (2004) and can be summarized in the following steps:

1. The conditions shown in Table 2 are used as the starting points of three stress method;
2. The operating conditions (SOR, SLR, RAS ratio, MLSS) shown in Table 2 are varied according to the stress test methods described previously;
3. The stress test ends with SST failure when the ESS exceeds 30 mg/L or when the sludge blanket height (SBH) rises to the effluent weir. The downward flow velocity (U_b) is calculated at the failure point and is called the limiting U_b.
4. The limiting U_b is then used to calculate the bulk flux and total flux of the 1DFT.
5. Steps 1–4 are performed for SSTs with and without the McKinney baffle.

The addition of the McKinney baffle improves SST performance, and the predicted limiting U_b increases for all conditions. Fig. 4 shows an example of the flux diagram for the original [Fig. 4(a)] and improved [Fig. 4(b)] SSTs, respectively. The limiting fluxes are estimated from the CFD simulations for Trial 1 in Table 2 using the first stress test method.

Results and Discussion

Tables 3–5 summarize the major results of the CFD stress tests, including (1) the limiting flux predicted by both the CFD modeling and the 1DFT analysis; (2) the limiting flux predicted by CFD as a percentage of the 1DFT limit; and (3) the failure reasons of SSTs, using the three stress methods. The starting points for each stress test method are the conditions shown in Table 2. Stress tests are performed with and without the McKinney baffle.

Stress Testing Using the First Method

Table 3 shows the predicted limiting fluxes, and the most obvious results are that the CFD analysis predicts much lower limiting fluxes than the 1DFT analysis. The addition of the McKinney baffle increases the predicted limiting flux using both methods, and the increases are substantial, increasing by 160%–200% for both methods; for example, the limiting flux increases from 8.3 to

Table 2. Main inputs for CFD stress tests

	Inflow parameters			Settling parameters			Dry solids density
Trial no.	MLSS (g/L)	RAS ratio	SOR (m/h)	V_o (m/h)	r_h (L/g)	r_p (L/g)	ρ_p (kg/m^3)
1	4.187	1.09	0.332	12.64	0.340	12.25	1,450
2	3.384	1.09	0.332	12.64	0.340	12.25	1,450
3	2.904	0.83	0.673	12.64	0.340	12.25	1,450

Note: V_o = stokes velocity; and r_h and r_p account for rapidly and poorly settling floc, respectively.

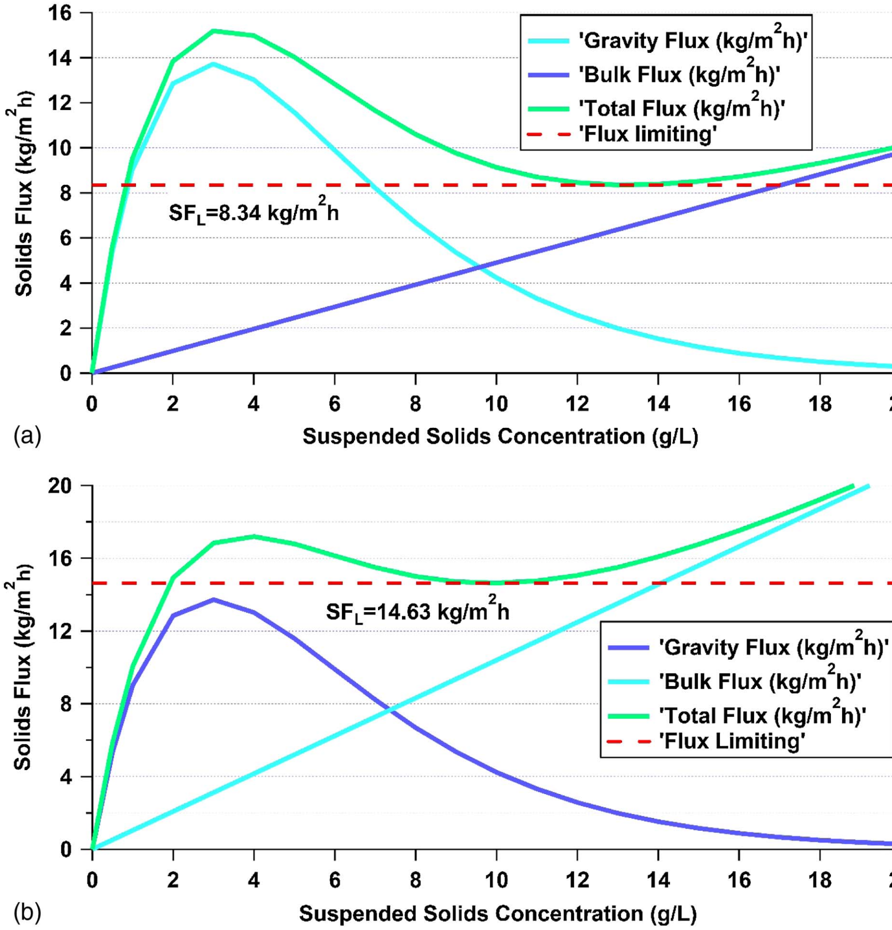

Fig. 4. Flux diagram for the SST (a) without the McKinney baffle; and (b) with the McKinney baffle. Flow conditions are initialized from Trial 1 and modified using the first stress test method.

Table 3. Summary of the limiting flux predicted by the 1DFT and CFD modeling using the first stress testing method (increasing Q with constant MLSS)

Trial no.	Presence of the McKinney baffle	SLR-1DFT $(kg/m^2\,h)$[a]	SLR-CFD $(kg/m^2\,h)$	SLR (%)	SOR[b] (m/h)	MLSS (g/L)	RAS ratio	Failure reason
1	No	8.3	3.9	47.2	0.45	4.187	1.09	Excessive carry over
	Yes	14.6	7.9	54.1	0.91	4.187	1.09	of SS by the upward
2	No	9.8	3.9	39.8	0.55	3.384	1.09	current toward the
	Yes	15.6	7.4	47.4	1.05	3.384	1.09	effluent weir
3	No	9.5	3.8	40.1	0.72	2.904	0.83	
	Yes	13.5	5.9	43.8	1.12	2.904	0.83	

[a]$1\ kg/m^2\,h = 0.2\ lb/(ft^2\,h)$.
[b]Limiting SOR used to calculate the limiting flux predicted by the 1DFT and CFD models.

Table 4. Summary of the limiting flux predicted by the 1DFT and CFD modeling using the second stress testing method (increasing Q with constant Q_r and MLSS)

Trial no.	Presence of the McKinney baffle	SLR-1DFT (kg/m^2h)[a]	SLR-CFD (kg/m^2h)	SLR (%)	SOR[b] (m/h)	MLSS (g/L)	RAS ratio[b]	Failure reason
1	No	6.6	3.5	52.5	0.47	4.187	0.75	Excessive carry over
	Yes	6.6	5.3	80.1	0.90	4.187	0.40	of SS by the upward
2	No	6.6	3.1	46.9	0.54	3.384	0.65	current toward the
	Yes	6.6	4.7	72.2	1.04	3.384	0.347	effluent weir
3	No	9.2	3.4	36.6	0.75	2.904	0.55	
	Yes	9.2	4.8	52.2	1.10	2.904	0.51	

[a]$1\ kg/m^2h = 0.2\ lb/(ft^2h)$.
[b]Limiting SOR and RAS ratio used to calculate the limiting flux predicted by the 1DFT and CFD models.

Table 5. Summary of the limiting flux predicted by the 1DFT and CFD modeling using the third stress testing method (increasing SLR as the MLSS increases)

Trial no.	Presence of the McKinney baffle	SLR-1DFT (kg/m^2 h)[a]	SLR-CFD (kg/m^2 h)	SLR (%)	SOR (m/h)	MLSS[b] (g/L)	RAS ratio	Failure reasons
2	No	6.6	5.2	80.0	0.33	7.6	1.09	A
	Yes	6.6	5.5	85.0	0.33	8.0	1.09	B
3	No	9.2	4.0	42.7	0.67	3.2	0.83	A
	Yes	9.2	6.6	71.0	0.68	5.3	0.83	A

Note: A = excessive carry over of SS by the upward current toward the effluent weir; and B = rising of sludge blanket to the effluent weir.
[a]1 $kg/m^2\,h = 0.2\ lb/(ft^2\,h)$.
[b]Limiting MLSS used to calculate the limiting flux predicted by the 1DFT and CFD models.

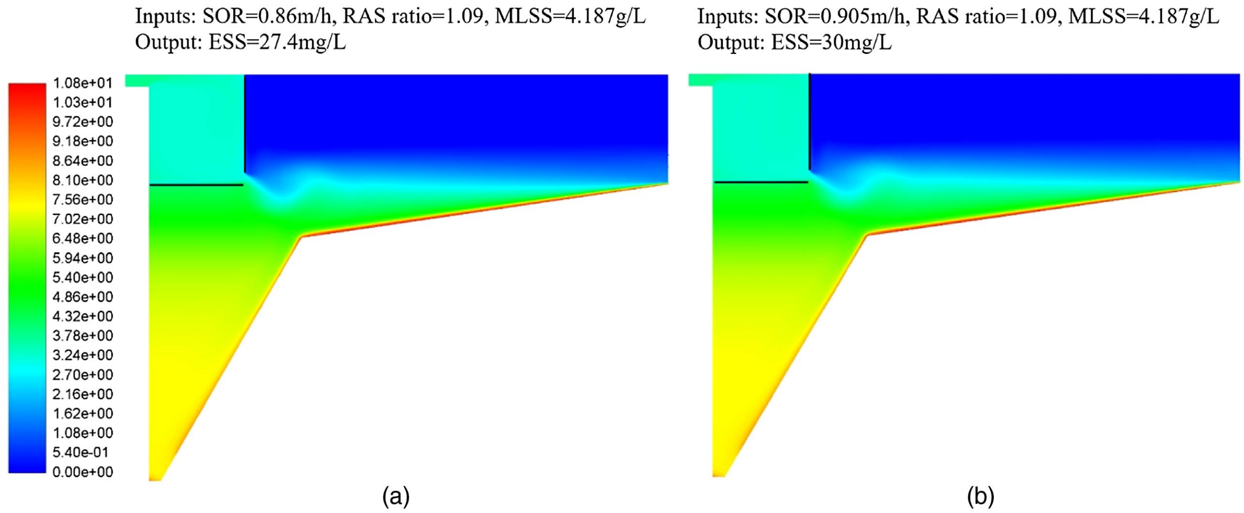

Fig. 5. Example concentration profiles (g/L) showing the acceptable SBH even when the ESS is excessive: (a) shows the last safe run; and (b) shows the first failure run using the first stress testing method.

14.6 kg/m^2 h or by 176% using the 1DFT analysis. There are still large differences in the predicted limiting fluxes between the 1DFT and CFD methods, but the percent differences are slightly less with the McKinney baffle for all three trials. For example, the CFD-predicted limiting flux is 47% of the 1DFT liming flux without the McKinney baffle and 54% with the McKinney baffle.

The failure mode for all three trials using the first stress testing method is the excessive ESS. In all cases the SBH is acceptable. Fig. 5 shows one example of acceptable SBH during the stress test even when the ESS is excessive. Fig. 5(a) shows the last safe run and Fig. 5(b) shows the first failure run using the first stress testing method. The 1DFT analysis does not conservatively predict ESS, which is understandable because the original goal of SST flux analysis was to predict thickening performance (Dick 1970).

Fig. 6 shows the predicted ESS calculated by CFD as a function of the SLR [$kg/(m^2\,h)$] for the first stress testing method. The most obvious result is the improvement provided by the McKinney baffle. Limiting flux increases from approximately 5.5 to 8.0 kg/m^2 h depending on the initial conditions. The trial number matters little for the results without the McKinney baffle, with all three trials having a limiting flux at approximately 4.0 kg/m^2 h. An interesting question is why do the different trials produce different limiting fluxes? Trial 3 produces the most conservative result whereas Trial 1 predicts the greatest SST capacity, and all trials fail because of excessive ESS. Trial 1 has the greatest MLSS concentration, and the higher influent MLSS creates a more compact, lower height SBH, which creates lower ESS. Therefore, if the stress test is conducted using the first stress test method, starting from a comparatively higher inlet MLSS concentration and lower influent flow rate will predict the greatest capacity.

Fig. 7 compares the velocity profiles for the original and modified SSTs under the limiting loading condition of the original SST. It shows that without the McKinney baffle [Fig. 7(a)], the density current forms a strong horizontal jet at the surface of the sludge blanket and flows upward to the effluent weir. Therefore, the original SST fails because of the excessive ESS stirred up from the surface of the sludge blanket to the effluent weir. With the addition of

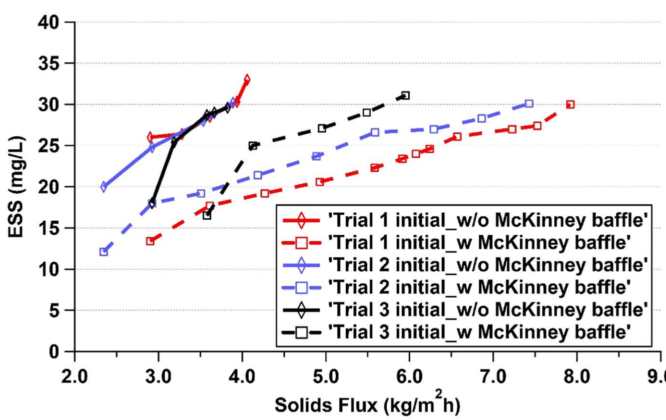

Fig. 6. ESS as a function of SLR [$kg/(m^2\,h)$] when CFD stress tests are conducted under the 1st operation method.

J. Environ. Eng., 2019, 145(10): 04019065

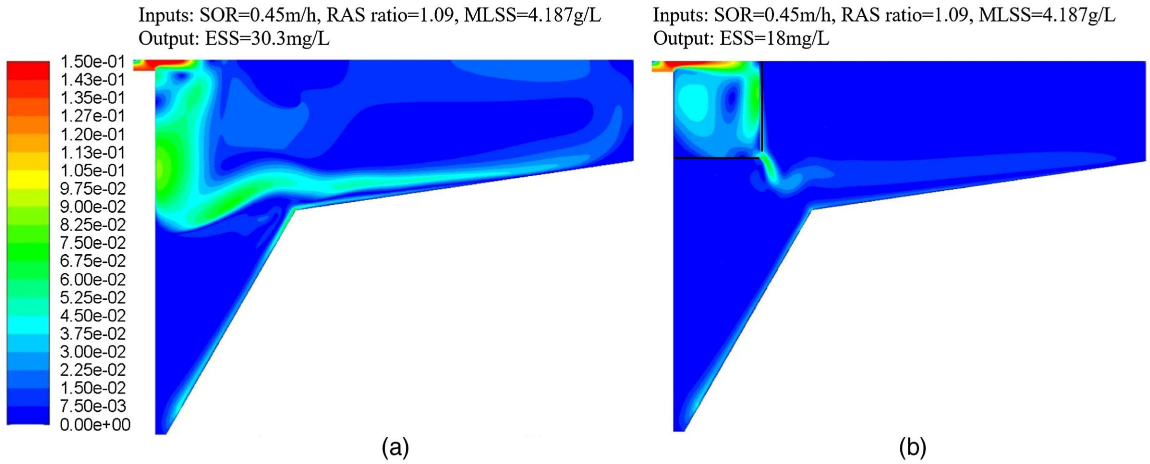

Fig. 7. Comparison of velocity profiles (m/s) for the (a) original and (b) modified SSTs when original SST fails because of clarification failure.

the McKinney baffle in the modified SST [Fig. 7(b)], inflow energy is significantly dissipated inside the inlet zone, and the horizontal jet outside the inlet zone is weakened. Therefore, the predicted ESS for the modified SST under the limiting loading conditions of the original SST is only 18 mg/L and the modified SST has larger capacity than the original SST with the addition of the McKinney baffle.

Stress Testing Using the Second Method

The second stress test method maintains a constant return flow rate (Q_r); therefore, the predicted 1DFT flux limit is the same for the original and improved SSTs. Therefore, the CFD predicted limiting flux as a percentage of 1DFT limit is proportional to the CFD predicted limiting flux and can be used to correctly describe the improvement of the modified SST. Table 4 shows that with the addition of McKinney baffle, the CFD predicted limiting flux as a percentage of the 1DFT flux limit is approximately 1.4–1.5 times as large for the SST without the McKinney baffle. It increases from 53%, 47%, and 37% to 80%, 72%, and 52%, when the stress test is initialized under the flow conditions of Trials 1–3, respectively. Among these six CFD predicted limiting fluxes, only the CFD predicted limiting flux initialized from flow conditions of Trial 1 for the modified SST reaches 80% of the 1DFT limit. The other five limiting fluxes are much lower than 80% of the 1DFT limit. Table 4 also shows that the maximum CFD predicted limiting flux [3.5 and 5.3 $\mathrm{kg/(m^2\,h)}$] are also reached by initializing with a comparatively higher inlet MLSS concentration and lower inflow rate, which is consistent to the results of stress tests using the first stress testing method.

Fig. 8 shows the prediction of the ESS as a function of the CFD predicted SLR [$\mathrm{kg/(m^2\,h)}$] tested using the second stress testing method. Similar to the results shown in Fig. 6, the prediction of ESS is gradually increased above 30 mg/L and the failure of SSTs is also caused by excessive carry over of SS by the upward current toward the effluent weir.

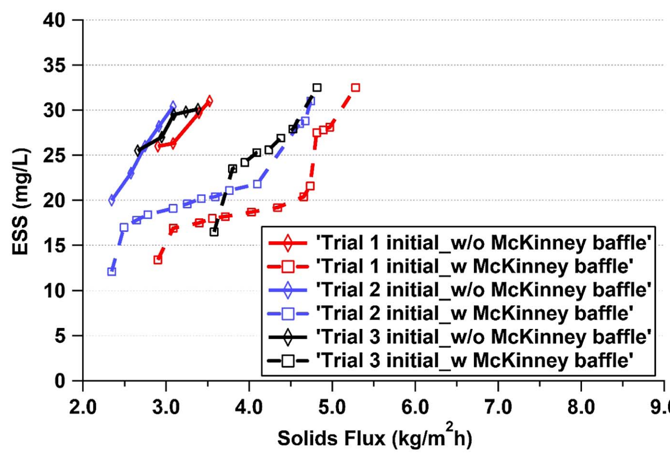

Fig. 8. ESS as a function of SLR [$\mathrm{kg/(m^2\,h)}$] when CFD stress tests are conducted under the 2nd operation method.

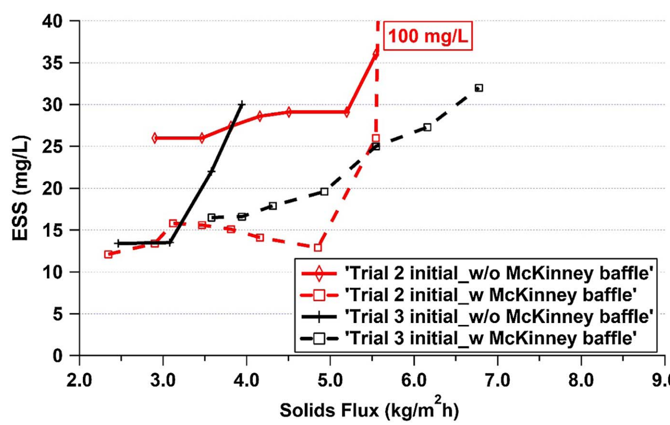

Fig. 9. ESS as a function of SLR [$\mathrm{kg/(m^2\,h)}$] when CFD stress tests are conducted under the 3rd operation method.

Stress Testing Using the Third Method

Because the flow conditions of Trials 1 and 2 are the same, except that the inlet MLSS concentration for Trial 2 is lower than in Trial 1, the stress test conducted on the third stress method is only started from the flow conditions of Trials 2 and 3. Also, since the Q_r remains constant when the stress test is started under the same flow conditions, the prediction of the 1DFT limit for the SSTs is the same. Therefore, describing the CFD predicted limiting flux as a percentage of the 1DFT limit can correctly evaluate the performance improvement of the SST.

Table 5 shows that the stress test conducted using the third stress testing method increases the CFD predicted limiting flux as a

J. Environ. Eng., 2019, 145(10): 04019065

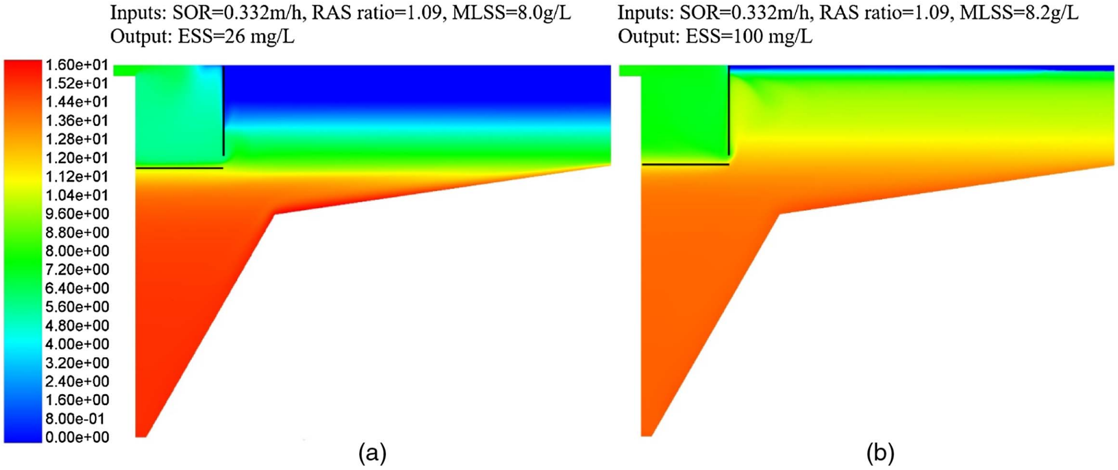

Fig. 10. Concentration profiles (g/L) showing the SST failure caused by rising of sludge blanket to the effluent weir: (a) the last safe run; and (b) the first failure run using the third stress testing method.

percentage of the 1DFT limit after the addition of the McKinney baffle. It increases from 80% and 43% to 85% and 71% when the stress test is initialized under the flow conditions of Trials 2 and 3, respectively. Among these four CFD predicted limiting fluxes, only the CFD predicted limiting flux initialized from flow conditions of Trial 2 for both SSTs reaches 80% of the 1DFT limit. Fig. 9 shows the prediction of the ESS as a function of the CFD predicted SLR $[\mathrm{kg}/(\mathrm{m}^2\,\mathrm{h})]$ tested on the third stress method. It shows that the failure of both SSTs is caused by clarification failure when the flow conditions of the stress test are initialized with Trial 3, whereas the failure of the original SST is caused by clarification failure while the failure of the modified SST is caused by solids overloading when the flow conditions of the stress test are initialized with Trial 2. Before the SST becomes solids overloaded, the performance of the SST is improved with an increase of the flux until a certain point (flux $= 5.4\ \mathrm{kg/m^2\,h}$), at which it starts to perform poorly until it suddenly fails by solids overload at $5.5\ \mathrm{kg}/(\mathrm{m}^2\,\mathrm{h})$.

When the modified SST is solids overloaded, the inlet MLSS concentration is as much as 8.2 g/L. Fig. 10 shows the concentration profiles for the modified SST under the last safe run and the first failure run initialized with flow conditions of Trial 2. It shows that the increasing of the inlet concentration of MLSS from 8.0 to 8.2 g/L causes the exaggerated rise of the sludge blanket to the water surface and the SST fails by solids overload.

Conclusions

In this study, effects of the McKinney baffle on the limiting flux of SSTs are studied on a Fluent-based CFD model. CFD stress tests are performed on three different stress testing methods. In each method, different flow conditions are used to initialize the stress test. The prediction of flux capacities of SSTs with and without the McKinney baffle are initialized with different flow conditions under each stress testing method. This study gives a detailed procedure to analyze the performance of the McKinney baffle and can be applied to study the effect of other internal geometries.

Compared with the prediction results of the stress test initialized with different flow conditions and conducted using different stress testing methods, only three of the ten CFD predicted limiting flux values (30%) reach 80% of the 1DFT limit under the 2nd and 3rd stress methods. Eighty percent of the 1DFT limit is reached for (1) the original SST without McKinney baffle when the CFD stress test is started with relatively higher inlet MLSS concentration and lower inflow rate (Trial 1), conducted using the 2nd stress method, and for (2) both original and modified SSTs when the CFD stress test is started with a higher inlet MLSS concentration and lower inflow rate (Trial 2), conducted using the 3rd stress method. Therefore, different internal baffling structures, initial flow conditions, and different stress testing methods all contribute to the CFD predicted limiting flux, and it is improper to use 80% reduction of the 1DFT for all SSTs.

Also, the prediction results of the stress test by using different stress methods (shown in Figs. 6, 8, and 9) indicate that the McKinney baffle significantly improves the performance of the SST. The predicted ESS for the modified SST with the McKinney baffle is at least 5 mg/L or 30% lower than the prediction of ESS for the original SST under every solid flux. Also, the addition of the McKinney baffle extends the SST limiting flux. The limiting flux in the modified SST can be approximately 1.4–2 times that of the original SST.

Additionally, because the limiting flux predicted by CFD model for the original SST without McKinney baffle is reached by conducting the CFD stress test using the third stress method (increasing MLSS alone), and the limiting flux predicted by CFD model for the modified SST with McKinney baffle is reached by conducting the CFD stress test under the first stress method (increasing flow rate alone), for an engineering consulting project, which is usually limited by the budget hours and does not have enough time to run many cases for CFD stress tests on SSTs with different geometries, it is recommended to increase the flow rate (Q) and MLSS alternatively, while keeping RAS ratio constant.

Based on the simulation results, the following conclusions are made:

1. The McKinney baffle greatly improves the limiting flux of an SST.
2. When stress testing an SST, a preferred strategy is to increase the inflow rate (Q) and MLSS alternatively, while keeping the RAS ratio constant.
3. Since initial flow conditions, internal geometries, and stress testing methods influence the prediction of the SST limiting flux, the limiting flux prediction ranges from approximately 36% to 80% of the 1DFT limit for the original SST, and ranges from approximately 43% to 85% for the modified SST; therefore, a flux rating of 80% of the 1DFT limit is not recommended

for all SSTs and evaluating the reduction rate of the 1DFT should be tested on a case-by-case basis.

References

Bokil, S. D. 1972. "Effect of mechanical blending on the aerobic digestion of the waste activated sludge." Ph.D. thesis, Dept. of Civil and Engineering, Univ. of Windsor.

Burt, D. J. 2010. "Improved design of settling tanks using an extended drift flux model." Ph.D. thesis, Dept. of Mechanical Engineering, Univ. of Bristol.

De Clercq, B. 2003. "Computational fluid dynamics of settling tanks: Development of experiments and rheological, settling, and scraper submodels." Ph.D. dissertation, Dept. of Applied Mathematics, Biometrics and Process Control, Univ. of Ghent.

Dick, R. I. 1970. "Role of activated sludge final settling tanks." *J. Sanitary Eng. Div.* 96 (2): 423–436.

Ekama, G. A., and P. Marais. 2004. "Assessing the applicability of the ID flux theory to full-scale secondary settling tank design with a 2D hydrodynamic model." *Water Res.* 38 (3): 495–506. https://doi.org/10.1016/j.watres.2003.10.026.

Gao, H., and M. K. Stenstrom. 2017. "Computational fluid dynamics applied to secondary clarifier analysis." In *Proc., World Environmental and Water Resources Congress 2017: Water, Wastewater, and Stormwater, Urban Watershed Management, and Municipal Water Infrastructure*, edited by C. N. Dunn and B. VanWeele, 301–315. Reston, VA: ASCE.

Gao, H., and M. K. Stenstrom. 2018a. "Evaluation of three turbulence models in predicting of the hydrodynamics of a secondary sedimentation tank." *Water Res.* 143: 445–456. https://doi.org/10.1016/j.watres.2018.06.067.

Gao, H., and M. K. Stenstrom. 2018b. "Turbulence and interphase mass diffusion assumptions on the performance of secondary settling tanks." *Water Environ. Res.* 91 (2): 101–110. https://doi.org/10.1002/wer.1003.

Gao, H., and M. K. Stenstrom. 2019. "Generalizing the effects of the baffling structures on the buoyancy-induced turbulence in secondary settling tanks with eleven different geometries using CFD models." *Chem. Eng. Res. Des.* 143 (Mar): 215–225. https://doi.org/10.1016/j.cherd.2019.01.015.

Keinath, T. M. 1985. "Operational dynamics and control of secondary clarifiers." *J. Water Pollut. Control Fed.* 57 (7): 770–776. https://doi.org/10.2307/25042697.

Keinath, T. M., D. A. Hofer, C. H. Dana, and M. D. Ryckman. 1977. "Activated sludge-unified system-design and operation." *J. Environ. Eng. Div.* 103 (5): 829–849.

Lakehal, D., P. Krebs, J. Krijgsman, and W. Rodi. 1999. "Computing shear flow and sludge blanket in secondary clarifiers." *J. Hydraul. Eng.* 125 (3): 253–262. https://doi.org/10.1061/(ASCE)0733-9429(1999)125:3(253).

Larsen, P. 1977. *On the hydraulics of rectangular settling basins: experimental and theoretical studies*. Lund, Sweden: Dept. of Water Resources Engineering, Lund Institute of Technology, Univ. of Lund.

McCorquodale, J. A., E. La Motta, A. Griborio, I. Georgiou, and J. Homes. 2004. *Development of software for modeling activated sludge clarifier system*. Technology Transfer Rep. New Orleans, LA: Univ. of New Orleans.

Parker, D. S., R. P. Merlo, J. A. Jimenez, and E. J. Wahlberg. 2008. "Analyzing wet weather flow management using state of the art tools." *Water Sci. Technol.* 57 (8): 1247–1251. https://doi.org/10.2166/wst.2008.217.

Patziger, M., H. Kainz, M. Hunze, and J. Jozsa. 2012. "Influence of secondary settling tank performance on suspended solids mass balance in activated sludge systems." *Water Res.* 46 (7): 2415–2424. https://doi.org/10.1016/j.watres.2012.02.007.

Ramalingam, K., S. Xanthos, M. Gong, J. Fillos, K. Beckmann, A. Deur, and J. A. McCorquodale. 2012. "Critical modeling parameters identified for 3D CFD modeling of rectangular final settling tanks for New York City wastewater treatment plants." *Water Sci. Technol.* 65 (6): 1087–1094. https://doi.org/10.2166/wst.2012.944.

Ramin, E., D. S. Wagner, L. Yde, P. J. Binning, M. R. Rasmussen, P. S. Mikkelsen, and B. G. Plosz. 2014. "A new settling velocity model to describe secondary sedimentation." *Water Res.* 66 (1): 447–458. https://doi.org/10.1016/j.watres.2014.08.034.

Rodi, W. 1993. *Turbulence models and their application in hydraulics*. Boca Raton, FL: CRC Press.

Takács, I., G. G. Patry, and D. Nolasco. 1991. "A dynamic model of the clarification-thickening process." *Water Res.* 25 (10): 1263–1271. https://doi.org/10.1016/0043-1354(91)90066-Y.

Tarpagkou, R., and A. Pantokratoras. 2013. "CFD methodology for sedimentation tanks: The effect of secondary phase on fluid phase using DPM coupled calculations." *Appl. Math. Modell.* 37 (5): 3478–3494. https://doi.org/10.1016/j.apm.2012.08.011.

Vitasovic, Z. C., S. Zhou, J. A. McCorquodale, and K. Lingren. 1997. "Secondary clarifier analysis using data from the clarifier research technical committee protocol." *Water Environ. Res.* 69 (5): 999–1007. https://doi.org/10.2175/106143097X125696.

Wahlberg, E. J., H. Z. Gerges, A. Gharagozian, M. K. Stenstrom, Z. Vitasovic, S. P. Zhou, J. A. McCorquodale, and K. Lingren. 1998. "Discussion of: 'Secondary clarifier analysis using data from the clarifier research technical committee protocol' by Z. C. Vitasovic, S. Zhou, J. A. McCorquodale, and K. Lingren." *Water Environ. Res.* 70 (2): 249–253. https://doi.org/10.2175/106143098X127107.

Wang, X., L. Yang, Y. Sun, L. Song, M. Zhang, and Y. Cao. 2008. "Three-dimensional simulation on the water flow field and suspended solids concentration in the rectangular sedimentation tank." *J. Environ. Eng.* 134 (11): 902–911. https://doi.org/10.1061/(ASCE)0733-9372(2008)134:11(902).

Water Environmental Federation. 2006. *Clarifier design*. 2nd ed., 507–540. New York: McGraw-Hill.

Xanthos, S., M. Gong, K. Ramalingam, J. Fillos, A. Deur, K. Beckmann, and J. A. McCorquodale. 2011. "Performance assessment of secondary settling tanks using CFD modeling." *Water Resour. Manage.* 25 (4): 1169–1182. https://doi.org/10.1007/s11269-010-9620-1.

Xanthos, S., K. Ramalingam, S. Lipke, B. McKenna, and J. Fillos. 2013. "Implementation of CFD modeling in the performance assessment and optimization of secondary clarifiers: The PVSC case study." *Water Sci. Technol.* 68 (9): 1901–1913. https://doi.org/10.2166/wst.2013.280.

Zhou, S., and J. A. McCorquodale. 1992a. "Influence of skirt radius on performance of circular clarifier with density stratification." *Int. J. Numer. Methods Fluids* 14 (8): 919–934. https://doi.org/10.1002/fld.1650140804.

Zhou, S., and J. A. McCorquodale. 1992b. "Mathematical modelling of a circular clarifier." *Can. J. Civ. Eng.* 19 (3): 365–374. https://doi.org/10.1139/l92-044.

Zhou, S., and J. A. McCorquodale. 1992c. "Modeling of rectangular settling tanks." *J. Hydraul. Eng.* 118 (10): 1391–1405. https://doi.org/10.1061/(ASCE)0733-9429(1992)118:10(1391).

Zhou, S., J. A. McCorquodale, and Z. Vitasovic. 1992. "Influences of density on circular clarifiers with baffles." *J. Environ. Eng.* 118 (6): 829–847. https://doi.org/10.1061/(ASCE)0733-9372(1992)118:6(829).